Adult somatic progenitor cells and hematopoiesis in oyster

Mohamed Jemaà[1], Nathalie Morin[1], Patricia Cavelier[2], Julien Cau[3], Jean-Marc Strub[4]
and Claude Delsert[5],*

[1] Universités Montpellier; CRBM CNRS UMR, France
[2] Universités Montpellier; IGMM CNRS UMR, France
[3] Universités Montpellier; IGH CNRS UPR, France
[4] Université de Strasbourg; IPHC CNRS UMR, France
[5] Universités Montpellier; CRBM CNRS UMR; IFREMER, France

*: Corresponding author : Claude Delsert, email address : claude.delsert@crbm.cnrs.fr

Abstract:

Long-lived animals show a non-observable age-related decline in immune defense, which is provided by blood cells that derive from self-renewing stem cells. The oldest living animals are bivalves. Yet, the origin of hemocytes, the cells involved in innate immunity, is unknown in bivalves and current knowledge about mollusk adult somatic stem cells is scarce. Here we identify a population of adult somatic precursor cells and show their differentiation into hemocytes. Oyster gill contains an as yet unreported irregularly folded structure (IFS) with stem-like cells bathing into the hemolymph. BrdU labeling revealed that the stem-like cells in the gill epithelium and in the nearby hemolymph replicate DNA. Proliferation of this cell population was further evidenced by phosphorylated-histone H3 mitotic staining. Finally, these small cells most abundant in the IFS epithelium were found positive for the stemness marker Sox2. We provide evidence for hematopoiesis by showing that co-expression of Sox2 and Cu/Zn SOD, a hemocyte-specific enzyme, does not occur in the gill epithelial cells but rather in the underlying tissues and vessels. We further confirm the hematopoietic features of these cells by the detection of Filamin, a protein specific for a sub-population of hemocytes, in large BrdU-labeled cells bathing into gill vessels. Altogether, our data show that progenitor cells differentiate into hemocytes in gill, which suggests that hematopoiesis occurs in oyster gills.

Keywords : Hematopoiesis ; Adult somatic ; Progenitor cells ; Hemocytes ; Mollusk ; Marine invertebrates

INTRODUCTION

The longest living animals belong to bivalves (Bureau et al., 2002; Peck and Bullough, 1993; Turekian et al., 1975; Ziuganov et al., 2000; Wanamaker et al., 2008; Butler et al., 2013), which are a main class among the mollusk phylum. Long-lived animals have been defined as non-senescing species (Finch and Austad, 2001) since they do not show any observable age-related decline in physiological capacity or disease resistance. Indeed, bivalves grow and most importantly they ensure their immune defense during their entire life (Bodnar, 2009). In bivalves, immunity involves both cell-mediated and humoral systems that operate in a coordinated way (for comprehensive reviews please see Pruzzo et al, 2005 and Schmitt et al, 2012). The cell-mediated immune defense is carried out by blood cells that are continuously produced in the adult animal and that derive from self-renewing populations of multipotent stem cells that are housed in specialized hematopoeitic organs (comprehensive review in Hartenstein, 2006). Yet, the origin of blood cells is unknown in bivalves (Vogt, 2012). Moreover our current knowledge about mollusk adult somatic stem cells is scarce. Mollusk cellular immunity is ensured by motile hemocytes (Cheng, 1996) circulating through the hemolymph before infiltrating tissues (Galtsoff, 1964; Eble and Scro, 1996). Three main types of hemocytes have been recognized in mollusks based upon their morphology, (i) granular cells with numerous cytoplasmic granulations, (ii) hyaline cells with a clear cytoplasm and (3i) rare and much smaller stem-like cells (Hartenstein, 2006; Cheng, 1996; Kuchel et al., 2011).

Yet, despite a long-standing interest in the bivalve immune system (Cuénot, 1891), the site of hematopoiesis as well as the relatedness between the different types of hemocytes, remain thorny questions in bivalves (Vogt, 2012; Kuchel et al., 2011). In another mollusk, *Biomphalaria glabrata*, an amebocyte-producing organ (APO) has been described based upon the observation in phase contrast microscopy of mitoses in the cardiac region (Jeong et al., 1983). Moreover, infestation by parasites appeared to increase the mitotic index of APO (Salamat and Sullivan, 2008) while other investigations (dos Santos Souza and Araujo Andrade, 2012) underlined the need for specific markers to characterize precursors and differentiated hemocytes in order to settle this matter in *Biomphalaria*.

Indeed, bivalves are not easily amenable to genetics, and while genomic data were published only recently (Zhang et al., 2012), these organisms are phylogenetically distant from main biological models. Meanwhile, farming of bivalves, a worldwide industry notably with the Pacific oyster *Crassostrea gigas*, is threatened by infectious diseases from viral, bacterial or protozoan etiology (Comps et al., 1976; Farley et al., 1972; Binesse et al., 2008; Cochennec et

77 al., 2003), which stresses the need for a better knowledge of the hemocyte biology. The origin

78 of hemocytes and consequently, the location of the hematopoietic organ thus remain a

79 fundamental question in bivalves. In particular, in regard to the key role played by hemocytes

80 in the cell-mediated immune defense (Duperthuy et al., 2011), and moreover, to the long-term

81 production and physiology of the yet-to-be-described mollusk stem cells that are essential to

82 the extreme longevity of certain bivalves (Butler et al., 2013).

83 Here we provide evidence for adult progenitor cells in bivalves and their differentiation into

84 hemocytes in the gill tissue. Analysis of the oyster gill revealed irregularly folded structures

85 (IFS) that displayed small round stem-like cells bathing into the hemolymph. BrdU labeling

86 revealed that the stem-like cells in the gill epithelium and in the nearby hemolymph actively

87 replicated DNA. Proliferation of stem-like cells was further evidenced in gill by the detection

88 of phosphorylated-histone H3, a mitosis marker (Minakhina et al., 2007). The existence of a

89 population of stem and /or precursor cells in oyster was established by the detection of Sox2,

90 a marker for stemness (Liu et al., 2013), particularly abundant in the IFS epithelial cells.

91 Hematopoiesis was evidenced by the co-expression of Sox2 and Cu/Zn SOD, a hemocyte-

92 specific enzyme (Gonzalez et al., 2005) in gill cells. Finally, hematopoiesis was confirmed by

93 the detection of Filamin (FLN), a protein specific for a sub-population of hemocytes (Rus et

94 al., 2006), in large BrdU-labeled cells bathing in the hemolymph of gill vessels. We thus

95 propose that gill is the long-searched for hematopoietic organ in bivalves (Cuénot, 1891).

96

97

98

99

100

101

102 **RESULTS**

103 **Stem-like cells exist in the gill epithelium and hemolymph**. The general structure of the

104 oyster gill (reviewed in Galtsoff, 1964; Eble and Scro, 1996) is briefly recalled here for the

105 purpose of this work, while further histological details are provided. The two oyster gills are

106 both made of two V-shaped demi-branches each composed of an ascending and a descending

107 lamella delimiting a water tube and linked by interlamellar junctions (Figs S1A, B). Each

108 lamella is a succession of regularly folded structures, termed plicas, which are made of the

109 repetition of a tubular structural unit called filament. The central part of the filament is

110 occupied by a space filled with hemolymph while the basal part of the filament consists of a

111 more or less regular layer of tightly-packed and non-ciliated cells referred to as the epithelium

112 (Galtsoff, 1964 ; Eble and Scro, 1996). Here, we examined in further detail the oyster gill

113 organization. Adult animals were collected during spring in the Mediterranean Sea. Scanning

114 of hematoxylin/eosin stained cross-sections using a Nanozoomer revealed intriguing

115 irregularly folded structures (IFS) in all the examined samples (n= 6) (Fig. S1C) in addition to

116 the regularly folded structures described above. IFS were found to be made of a succession of

117 stacks of 8 or less, long and thin parallel structures next to irregular folds, here referred to as

118 tubules and convoluted structures, respectively (Figs 1A, S1B). The term epithelium is here

119 conserved for the cell layer delimiting these structures since it defines the limit between the

120 body and its environment, despite the fact that its organization does not correspond to a

121 classical epithelial cell lining. Hematoxylin staining was intense in the epithelium and at the

122 extremities of all tubules (Fig. 1A), which indicated a high concentration of nucleic acids. At

123 higher magnification nuclei appeared as densely packed and surrounded by a thin and barely

124 detectable eosin-stained cytoplasm (Fig. 1A, insets). The IFS epithelium is thus an irregular

125 layer of cells, associated in tight groups and embedded in a thick extra cellular matrix (ECM)

126 as shown on eosin-stained sections (Fig. 1A). The convoluted structures are less compact (Fig.

127 1B, C) and they are better suited to study the interaction between the epithelium and its

128 environment. Taking advantage of the lesser density of IFS, observation revealed small cells

129 with a pear-shape nucleus, displaying no visible cytoplasm, which are morphological traits of

130 stem cells (Rink, 2013). Some of these cells were barely attached to the tissue as if being

131 released from the epithelial ECM into the hemolymph (Fig. 1B, inset, arrow). In addition,

132 small cells with long and thin cytoplasmic extensions protruding inside the tubules lumen (Fig.

133 1C, inset, arrow) were also observed in IFS. Interestingly, cytoplasmic protrusions are

134 generally considered as an indication of cell movement (Lauffenburger and Horwitz, 1996).

135 **Intense DNA replication occurs in the gill epithelium and hemolymph cells.** One main

136 characteristic of the hematopoietic tissue is to sustain a high level of DNA synthesis as

137 exemplified by the drosophila larval lymph gland (Jung et al., 2005).

138 To determine whether gill is the site of intense DNA synthesis, entire gills (n= 3) were cut out

139 while preserving their superficial attachment region to the body. 10 mm-thick cross-sections

140 of the isolated gill were incubated for 16 hrs in L15 cell culture medium adjusted to seawater

141 osmolarity and containing BrdU (25 µM), a nucleotide analog, before immediate fixation.

142 Paraffin cross-sections were submitted to immunohistochemistry (IHC) using a commercial

143 mouse monoclonal anti-BrdU antibody. Fluorescence microscopy (Cy3) revealed a

144 punctuated labeling typical of the DNA-incorporated BrdU in gill (Fig. 2). Labeling was

5

145 particularly intense in the epithelium of the IFS tubules and convoluted structures (Fig. 2A, 1-

146 2) but also in areas of the regular folds and the adjacent inter-lamellar junctions (Fig. 2A, 3-5)

147 while no signal was detected on control sections (Fig. 2A, 6).

148 To determine whether DNA synthesis is more intense in gills than in other tissues, a solution

149 of BrdU (1.6 mM L^{-1}) was administered by injection to spats (n= 3) for 6 hours before

150 fixation of the entire body of the animals. Fluorescence microscopy (Cy3) revealed BrdU

151 labeling (Fig. S2, panels BrdU) while autofluorescence was recorded in the GFP channel

152 (panels AF) to outline the tissues. The specificity of BrdU labeling was assessed by the

153 absence of staining when primary antibody was omitted (Fig. S2B, D, F). The examination at

154 low magnification indeed showed that BrdU-labeling was more intense in the IFS (Fig. S2A)

155 and in areas of the regularly folded gill (Fig. S2C) than in the mantle (Fig. S2E).

156 To further verify that BrdU-incorporation corresponded to DNA synthesis and not to DNA

157 reparation, the amount of cellular DNA was estimated using FACS analysis, which allows the

158 distinction between cells in G0 or G1phase and cells replicating DNA (S phase) or sustaining

159 mitosis (G2/M) (Vitale et al., 2013). FACS analysis (Fig. S3A) of the cells dissociated from

160 oyster (n= 6) gills and mantles, following enzymatic incubation of minced tissues, revealed a

161 higher percentage of S and G2/M phases in the gill (17.3%) that in the mantle (7.2%) (Fig.

162 S3B, C). Moreover, cell counting revealed that cells dissociated from gill were 6.3 fold more

163 numerous than for mantle (Table S1), which together with the gill higher mitotic index (2.40

164 fold) indicate that the number of cells proliferating is much greater in gill (15 fold) than in

165 mantle. This quantitative data is in agreement with the higher rate of BrdU incorporation

166 observed on gill sections (Figs 2A and S2A, C) and it indicates that indeed BrdU

167 incorporation essentially corresponded to DNA synthesis.

168 Gill cross-sections, treated as above, were co-stained with fluorescent Phalloidin, which binds

169 the F-actin and thus indicates the cytoplasm extent. Confocal microscopy revealed thin

170 fluorescent rings around abundant BrdU-labeled nuclei in both the tubule epithelium and

171 lumen (Fig. 3A), thus indicating that these stem-like cells undergoing replication in the IFS

172 are almost devoid of cytoplasm. Observation at higher magnification (Fig. 3B, enlarged Box

173 of Fig. 3A) revealed small oblong stem-like cells massed in a tubule lumen (outlined by white

174 lines). These cells appeared to be lined up in the direction of a less crowded part of the lumen

175 (Fig. 3B, broken line). Interestingly, examination of a nearby sinus (Fig. 2B, outlined)

176 revealed heterogeneity in the BrdU-labeled cells bathing in the hemolymph, which sizes

177 spread from the small stem-like cells (arrow head) to what could be large hemocytes (arrow).

178 This data suggests that cells that incorporated BrdU may later differentiate into hemocytes

6

179 since hemocytes do not replicate DNA (Hartenstein, 2006). To study this interesting

180 possibility, gill cross-sections were labeled with BrdU for a short period of time (2 hrs) and

181 immediately fixed and submitted to IHC as above. Under these conditions, a clearly

182 detectable BrdU signal was again observed in the stem-like cells inside the lumen of a sinus

183 (Fig. 3C, arrow heads). But in contrast, under these conditions no BrdU labeling was detected

184 in the surrounding large hemocytes (Fig. 3C, arrows).

185 This result shows that, as expected, the large hemocytes did not incorporate BrdU during the

186 two hours incubation. Furthermore, it strongly suggests that the BrdU positive stem-like cells

187 could differentiate into hemocytes, explaining the existence of a BrdU positive hemocyte

188 population following a long BrdU incubation (Fig. 2B, arrow).

189

190 **Cells proliferate in the gill epithelium and hemolymph.** Cell proliferation is a distinctive

191 feature of the lymph gland tissue in adult animals (Parslow et al., 2001). Cell proliferation

192 was assayed using a commercial antibody against the phosphorylated (Ser10) histone H3

193 (H3PAb), a widely used mitosis marker, notably in drosophila (Minakhina et al., 2007).

194 Specificity of H3PAb for the oyster H3P was assayed on an immunoblot carrying gill

195 chromatin extracts, which revealed a unique band corresponding to the expected molecular

196 weight for the oyster histone H3 (15 kDa; EKC28030), while no band was observed on the

197 corresponding non-chromatin supernatant (Fig. S4A).

198 IHC was carried out on cross-sections of oysters (n= 3) using H3PAb and DAPI to stain DNA.

199 Confocal images revealed H3P-positive nuclei in both mantle (Fig. 4A) and gill (Fig. 4B),

200 although H3P signal appeared much more abundant in the gill, while it was absent in the

201 negative control (Fig. 4C). For quantification, contiguous confocal microscope fields were

202 recorded at low magnification (x 20) and counted for H3P and DAPI in both mantle and gill

203 (Tables S2, S3).

204 The percentage of H3P-positive cells was quite high for gills (21.8%) when compared to

205 mantles (4.7%) (Fig. 4 D) (n= 3). Moreover, measurement of the tissue surface in the

206 corresponding microscope fields, using the ImageJ software, provided density values of 0.192

207 and 0.005 H3P-positive nuclei per 100 μm^2 for gill and mantle, respectively (Fig. 4E). Thus

208 the gill higher cell density and mitotic index show that more cells divide in gill than in mantle.,

209 which confirms the indirect evidence by FACS analysis (Fig. S3).

210

211 **Stem and/or precursor cells are abundant in the gill.**

212 Stem and precursor cells express specific markers such as the transcription factor Sox2 (Liu et

213 al., 2013). A commercial anti-Sox2 antibody specifically revealed a unique band migrating

214 according to the oyster Sox2 predicted molecular weight (EKC24855, 36 kDa) on an

215 immunoblot carrying oyster gill extract (Fig. S4B). IHC was carried out on gill cross-sections

216 using Sox2 antibody and DAPI. Confocal microscopy revealed a striking abundance of Sox2-

217 positive nuclei in gill (Fig. 5A), in particular, as shown at higher magnification, on cells

218 clustered in the IFS epithelium (Fig. 5B, Ep). Moreover, Sox2 was found decorating loosely

219 associated cells (Fig. 5C, stars) that filled the tubules lumen (Fig. 5C, Lu), in a similar way to

220 the groups of stem-like cells observed through histology (insets in Fig.1, B, C) or BrdU

221 labeling (Fig. 3B).

222 Altogether our data show that gill contains an abundance of stem and/or precursor Sox 2

223 positive cells, some of which localized into the hemolymph.

224

225 **Progenitor cells differentiate into hemocytes in gill.** IHC was performed on cross-sections

226 using Sox2 antibody and a mouse antibody against the Zn/Cu Superoxide Dismutase (SOD),

227 an enzyme that is specifically expressed in the oyster hemocytes (Duperthuy et al., 2011;

228 Gonzalez et al., 2005). The epithelial cells of the IFS tubules (Fig. 6A, Tu) were intensely

229 labeled for Sox2 as seen above while fewer cells were labeled in the rest of the tissue (Figs

230 6A and S5). By contrast, and very strikingly SOD-labeled cells were mostly restricted to the

231 vessel adjacent to the tubules (Figs 6A and S5). We emphasize from these data that cells that

232 are co-stained for Sox2 and SOD are likely to be progenitors (Sox2-positive) differentiating

233 into hemocytes (SOD-positive). The fact that the co-stained cells are not localized in the

234 tubule area (Tu) but mostly in the underlying connective tissue (Co) and vessels (V) (Figs 6A

235 and S5) suggests that progenitors may migrate from the tubules towards the IFS vessel. This

236 striking distribution of Sox2 and SOD markers is a general feature of the IFS structures as

237 further shown at lower magnification on Fig. S5.

238 To confirm that gill precursors differentiate into hemocytes, another hemocyte marker,

239 Filamin (FLN), was used. Indeed, this large actin binding protein is specific for a subclass of

240 hemocytes carrying out the encapsulation of parasites in drosophila (Rus et al., 2006), the

241 lamellocytes. Interestingly, encapsulation has also been described in mollusks (Loker and

242 Bayne, 2001). The oyster FLN was purified to homogeneity (Fig. S6A) and its identity was

243 confirmed through mass spectrometry (Table S4). A rabbit antibody was raised and immuno-

244 purified (FLNAb) against the FPLC-purified oyster protein. Specificity of FLNAb was shown

245 by an immunoblot using gill extract (Fig. S4C) that revealed a protein migrating well over the

246   250 kDa marker, which is in agreement with the oyster FLN molecular weight (323 kDa;

247   EKC28512.1).

248   IHC was performed on oyster cross-sections using FLNAb, SODAb and DAPI. Confocal

249   microscopy confirmed FLNAb specificity since it revealed an intense and specific signal in

250   the gonad axillary cells (Fig. S6B) as previously shown for drosophila (Sokol and Cooley,

251   2003). Furthermore, confocal microscopy revealed a sub-population of cells bathing into the

252   IFS sinuses and vessels, which were confirmed to be hemocytes for their SOD co-labeling

253   (Fig. S6C).

254   Using this tool, we addressed whether gill precursors indeed differentiate into hemocytes.

255   Thick cross-sections of gill tissue were incubated for 16 hrs with BrdU as above and

256   immediately fixed. IHC was then carried out on gill cross-sections using first the FLNAb and

257   then after acidic denaturation, the anti-BrdU mAb. Fluorescence microscopy revealed strong

258   signals for both FLN and BrdU in cells bathing in the hemolymph, notably of a main gill

259   blood vessel (Fig. 6B, C).

260   This latter result is particularly significant since it shows that the stem and/or precursor cells

261   replicated DNA and differentiated into hemocytes expressing the FLN marker, in this isolated

262   piece of the oyster gill.

263

264   **DISCUSSION.**

265   The aim of this research was to address the origin of hemocytes in bivalve. This question was

266   complicated by the fact that the existence of adult somatic progenitor cells had not been

267   shown.

268   In bivalves, immunity involves both cell-mediated and humoral systems. While the effectors

269   of the humoral defense, including soluble lectins, lysosomal enzymes (e.g. acid phosphatase,

270   lysozyme) and anti-microbial peptides (Gueguen et al., 2006 and 2009; Gonzalez et al.,

271   2007a, b; Rosa et al., 2011), are synthesized by both hemocytes and epithelial cells (Itoh et al.,

272   2010, Xue et al., 2010), the cell-mediated immune defense is exclusively performed by

273   hemocytes (reviewed in Schmitt et al., 2012). Indeed, hemocytes are capable of non-self

274   recognition, chemotaxis, and active phagocytosis (Cheng, 1981). Moreover, hemocytes are

275   implicated in cytotoxic reactions by the production of hydrolytic enzymes (Cheng and

276   Rodrick, 1975), ROS (Bayne, 1990; Pipe, 1992; Lambert et al., 2007; Aladaileh et al., 2007;

277   Butt and Raftos, 2008; Boulanger et al., 2006; Kuchel et al., 2010) and antimicrobial

278   peptides/proteins (Gueguen et al., 2006, 2009; Gonzalez et al., 2007a, b; Rosa et al., 2011)

279   and phenoloxidases, a class of copper proteins involved in melanization, an immune defense

9

280   reaction associated with the encapsulation of larger parasites (Luna-Acosta et al., 2011).

281   Beside their immunological functions, mollusk hemocytes are believed to be involved in shell

282   mineralization (Mount, 2004), excretion, metabolite transport and digestion and wound repair

283   (reviewed in Cheng, 1996).

284   Yet, despite the multiple hemocyte functions that have been studied, the origin of hemocytes

285   in bivalves has remained elusive since L. Cuénot (1891) published his founding work on the

286   origin of blood cells in animals. Even more striking is the fact that, although mollusks are

287   models for a spectrum of research including frontier science in neurobiology (Landry et al.,

288   2013) or ageing (Philipp and Abele, 2010), little is known about mollusk adult somatic stem

289   cells. Recently, Vogt (2012) while reviewing on the invertebrate stem cells revived the

290   question of the existence and most importantly of the long-term protection of stem cells in the

291   extremely long-lived bivalves (Philipp and Abele, 2010).

292   Here we reexamined the origin of bivalve hemocytes by scrutinizing the adult oyster tissues

293   and by identifying markers for both bivalve progenitor cells and hemocytes. While focusing

294   on the gill for its overall higher density of nuclei as shown through histology and IHC, a less

295   dense structure termed IFS was uncovered, which contains a population of small stem-like

296   cells (Fig. 1). Interestingly, although IFS occupies a variable proportion of the gill (1/6 to

297    $1/5^{th}$ of a gill section), it was consistently highlighted in IHC when using markers for cell

298   proliferation or for stemness, which emphasizes the IFS contribution to precursor cell

299   proliferation in gills. In addition, histology suggested that a fraction of stem-like cells were

300   only loosely attached to the IFS epithelium while in other places they produced long

301   protrusions inside the tubules. Interestingly, these cytoplasmic extensions are usually

302   recognized as indicative of cell motion (Lauffenburger and Horwitz, 1996). Therefore, the

303   stemness traits of these small cells in contact with the hemolymph, raised the possibility they

304   participated to the oyster hematopoiesis.

305   Hematopoiesis requires precursor cell proliferation as exemplified by the daily production of

306   10^{11} blood cells in human adults. The production of hemocytes can be deduced from the

307   hemocyte population size and half-life. Indeed, the complete blood collection of an

308   experimental oyster (10 grams of meat) routinely provides 10^6 hemocytes (Rolland et al.,

309   2012), which is a conservative value since the proportion of blood cells infiltrating the oyster

310   tissues is unknown. On the other hand, the hemocyte half-life was determined to be 22 days

311   for the related American oyster *C. virginica* (Feng and Feng, 1974), a value consistent with

312   the 28 days found for another bivalve, *Mercenaria mercenaria* (McIntosh and Robinson,

313   1999). Based upon these values, the lower range for the daily loss of hemocytes can be

10

314   estimated at 22.000 h/d for a middle-size individual. As a matter of fact, several lines of

315   evidence corroborate this observation. First, the importance of apoptosis in the functioning of

316   the mollusk immune system is reflected by the detection of high baseline apoptosis rates that

317   range from 5 to 25 % in circulating hemocytes and can reach to up to 50 % in infiltrating

318   tissue hemocytes (Sunila and LaBanca, 2003; Sokolova et al., 2004; Goedken et al., 2005;

319   Cherkasov et al., 2007). This high rate of apoptosis is tied to the immune defense against

320   parasites and pathogens but also against toxic environments. Both *in vivo* and *in vitro*

321   infections were shown to result in hemocyte phagocytosis, respiratory burst and finally in

322   apoptosis (Goedken et al., 2005). On the other hand, detoxification of environmental

323   pollutants, including of toxic substances produced by harmful algal blooms, has been shown

324   to induce massive apoptotic death among the hemocyte population in bivalves (Medhioub et

325   al., 2013; Ray et al., 2013; Yao et al., 2013; Prado-Alvarez et al., 2013). In addition, a

326   physiological process not related to immune defense, shell mineralization, also lead to an

327   important loss of hemocytes since it requires the migration of numerous hemocytes to the

328   surface of the shell-facing outer mantle epithelium (Mount et al, 2004). A high capacity of

329   hemocytes production is therefore expected in oysters and most likely in other bivalves.

330   DNA replication, here used as an indicator of cell division, was shown through BrdU-labeling

331   (Figs 2 and S2) to be at a higher rate in gill than in mantle, another main tissue. Moreover, the

332   percentage of cells with a DNA content indicative of cells engaged in division was also

333   significantly higher in gill than in mantle as shown by FACS analysis (Fig. S3).

334   Cell proliferation was confirmed in gill using the histone H3P, a mitotic marker. Indeed,

335   counting the H3P-positive versus DAPI nuclei on confocal cross-sections confirmed that gill

336   cells have quite a higher mitotic index than mantle. Furthermore, the higher cell density in gill

337   than in mantle, a lacunar tissue (Galtsoff, 1964; Eble and Scro, 1996), translates into a much

338   higher density of dividing cells in gill than in mantle (Fig. 4E). Gill therefore appears to have

339   a superior capacity of generating cells.

340   In healthy adults, cell proliferation is likely to occur only in the hematopoietic organ in which

341   blood cell progenitors are expected to be abundant. Indeed, the striking abundance of Sox2-

342   positive cells in gill, notably in the IFS epithelium and hemolymph (Fig. 5) confirmed our

343   initial hypothesis that the small round cells with a pear-shape nucleus seen through histology

344   (Fig. 1), were stem or progenitor cells. Together these data demonstrate the existence of adult

345   somatic progenitor cells in mollusk, a prerequisite for hematopoiesis (Hartenstein, 2006).

346   Interestingly, cells that proliferate or express Sox2 in the IFS hemolymph mostly belong to

347   groups of loosely associated cells (Figs 3B and 5C), which is reminiscent of the electron

348   microscopy description of the hematopoietic clusters of the Polychaete annelid *Nicolea*

349   *zostericola* (Hartenstein, 2006; Eckelbarger, 1976).

350   In addition, the IFS epithelium is embedded in a thick eosin-stained ECM from which stem-

351   like cells emerge (Fig. 1). It is noteworthy that the epithelial ECM is a major component of

352   the stem cell niche (reviewed in Watt and Huck, 2013). Indeed, it was recently shown that the

353   alteration of the lymph gland ECM, due to the loss of the proteoglycan Perlecan/troll, reduces

354   the proliferation of progenitor cells in drosophila (Dragojlovic et al., 2013; Grigorian et al.,

355   2013).

356   Interestingly SOD, a hemocyte-specific enzyme (Duperthuy et al., 2011; Gonzales et al.,

357   2005), revealed an intriguing IFS spatial partition between the Sox2-positive stem and/or

358   progenitor cells in the tubules and the hemocytes in the underlying vessels (Figs 6A, S5).

359   Moreover, cells co-labeled for Sox2 and SOD are also mostly in the underlying connective

360   tissue and vessels. This striking partition suggests that the Sox2-positive progenitor cells

361   might differentiate into hemocytes while moving towards the gill vessels.

362   FLN, a large protein expressed in drosophila lamellocytes, hemocytes that are involved in the

363   defense against parasites (Rus et al., 2006; Sokol and Cooley, 2003), was shown to

364   characterize a sub-population of oyster hemocytes (Fig. S6C). Interestingly, the recent finding

365   that FLN RNA is overexpressed in the hemocyte population of oysters infested with parasites

366   (Morga et al., 2011) suggests that the FLN-positive hemocytes might indeed be lamellocytes.

367   The FLN marker was used to further show that an isolated piece of oyster gill constitutes a

368   biological system in which progenitor cells can replicate DNA and differentiate into

369   hemocytes (Fig. 6B, C), thus unambiguously showing that hematopoiesis occurs in gill.

370   Therefore, we believe that altogether our data show that gill is a significant contributor to the

371   oyster hematopoiesis.

372   While the evidence for adult somatic stem cells provided by this work should have an impact

373   on mollusk biology as it did in other biological systems, a direct implication of these findings

374   is expected on studies including (i) the maintenance of stem cells in extremely long-lived

375   bivalves (2i) the life-long growth of tissues in bivalves and graft in pearl oysters (3i) the

376   mollusk neoplasia notably in farmed bivalves (4) the development of mollusk continuous cell

377   culture.

378

379

380

MATERIALS AND METHODS

381

Animals and hemolymph collection. Adult *C. gigas* (15-20 g of meat) and spat (1.8 g of
meat) were purchased from local oyster farms in Palavas-les-Flôts (Gulf of Lion, France).

384

Reagents

All chemicals were from Sigma Aldrich (St. Louis, MO, USA) unless otherwise mentioned.

387

Histochemistry and IHC. Tissues were fixed using Davidson's fixative [for 1 liter: 330 mL
95% ethyl alcohol, 220 mL 37% Formaldehyde solution, 115 mL glacial acetic acid, 335 mL
filtered sea water] at 4°C for 16 hours. Tissue samples were then dehydrated in 70%, 80% and
96% successive ethanol bathes and then twice in Xylene before embedding in paraffin. 5µm
thick cross-sections were cut using a HM355S microtome (Thermoscientific, Illkirch, France)
and then dried O/N at 37°C. Paraffin was eliminated in Xylene bathes and sections were then
rehydrated in successive 96% to 70% ethanol bathes and then in TBST (50 mM Tris (8.0),
150 mM NaCl, 0.05% Tween 20).

For histology, tissue slides were incubated with Hematoxylin for 2 mn and then
counterstained for 4 mn with Eosin G (0.5% Ethanol), and washed in 100% ethanol and
xylene before mounting in Mountex medium (Histolab, Seoul, Korea).

For IHC, sections were permeabilized for 1 hour in 0.2% Triton in TBST solution containing
5% fat free milk. Sections were incubated with primary antibodies diluted in 2% Bovine
Serum Albumin in TBST overnight in a humid chamber at 4°C.

During co-detection of protein and BrdU, BrdU was detected in a second step. After protein
revelation with fluorescent secondary antibody, a 2M HCl denaturation step was carried out
for 30 mn at 37°C before instant renaturation using 0.1 M Borax (pH 9.0) and several rinses
in TBST, before O/N incubation at room temperature with anti-BrdU monoclonal antibody.

Antibodies and Immunopurification. Antibodies characteristics and dilution: Monoclonal
anti-BrdU (B-8434, IgG1) from Sigma (Saint Louis, Mo, USA) at dilution 1/500; Rabbit
polyclonal anti-H3P (06-570, immuno-purified) from MerckMillipore (Darmstadt, Germany)
at dilution 1/1000; Rabbit polyclonal anti-Sox2 (ab97959, immuno-purified) from Abcam
(Cambridge, MA, USA) at dilution 1/1000; In house mouse monoclonal anti-SOD (immuno-
purified) was used at dilution 1/1000 (Gonzalez et al., 2005); In house rabbit polyclonal anti
FLN antibody: Ammonium Sulfate pellets containing oyster FLN purified as described in
Materials and Methods, were injected to a rabbit. For immuno-purification, purified FLN was

414 covalently bound to CNBr-activated Sepharose™ 4 Fast Flow according manufacturer's

415 recommendation. Immunopurification was performed as previously described (Cau et al.,

416 2001). Immuno-purified FLN antibody was used at dilution 1/1000. All the secondary

417 antibodies were prepared from affinity-purified goat antibodies that react with IgG heavy

418 chains and all classes of immunoglobulin light chains from rabbit or mouse (Molecular

419 Probes, Eugene, Oregon, USA): Goat anti-rabbit Alexa 555 (A21429) at dilution 1/1000;

420 Goat anti-mouse Alexa 488 (A11029) at dilution 1/1000. To reveal the rabbit anti H3P, a

421 biotinylated goat anti-rabbit (S323555) was used at dilution 1/500 and revealed using Avidin

422 Alexa 647 (S21374, Molecular probes) at dilution 1/1000. Secondary antibodies were

423 incubated at room temperature for 1 hour. When necessary, DAPI (Sigma, D8417) was added

424 at dilution 1/3000 to the secondary antibody. Mounting medium for fluorescence microscopy

425 was made as follows: 10 g of Mowiol (Sigma, 81381) and 2.5 g of DABCO (Sigma, 290734)

426 were dissolved in 90 mL PBS (pH 7.4) and 40 mL glycerol were added. 500 µl aliquotes were

427 frozen at -20°C until use.

428 **BrdU incorporation.** 100 µl of a 1.6 mM BrdU solution was injected in the sinus of the

429 adductor muscle of oysters (1.8 g of meat, n= 3), which were maintained in seawater at room

430 temperature for 6 hours before fixation of the entire body. Alternatively, thick body cross-

431 sections were incubated as follows: one transversal section was carried out on the hedge of

432 the heart chamber while the other parallel section was 10 mm away in the direction of the

433 mouth (Galtsoff, 1964). Tissue sections were incubated in 50 mL of L15 cell culture medium

434 (LifeSciences Invitrogen, Grand Island, NY, USA) adjusted to 1100 mOsm with sea salts and

435 supplemented with 25 µM mL^{-1} BrdU (B5002, Sigma Aldrich) under mild stirring at 15°C for

436 various lengths of time. Note that the BrdU concentration is low compared to the conditions

437 used for mouse *in vivo* labeling (160 µM Kg^{-1} of tissue) (Magavi et al., 2008).

438 **FACS analysis.** The entire mantle and gills were harvested from oysters (15-20 g of meat,

439 n=6). Tissues were minced and incubated with Pronase (20 µg mL^{-1}) in 1100 mOsm-Hank's

440 buffer containing no Ca^{2+} or Mg^{2+} with a gentle shaking overnight at 4°C. Supernatant was

441 filtered (50 µm mesh) and debris were eliminated by several washes and centrifugations at

442 low speed (100 g) in Hank's buffer at 4°C for 10 mn. Cells were then fixed on Davidson's

443 fixative for 20 mn at room temperature and washed in PBS after centrifugation at 100 g for 10

444 mn. Pellets were resuspended in Propidium Iodide (50 µg mL^{-1}) in 0.1% (w/v) D-glucose in

445 PBS supplemented with 1 µg mL^{-1} (w/v) RNAse A and incubated for 30 min at 37°C and then

446 overnight at 4°C. FACS acquisitions were performed using a FACSCalibur (BD Biosciences,

447 San Diego, CA, USA) equipped with a 70 µm nozzle and data were statistically evaluated

448   using the CellQuestTM (Becton Dickinson, Pont de Claix, France). Only the events

449   characterized by normal forward scatter (FSC) and side scatter (SSC) parameters were gated

450   for inclusion in the statistical analysis (Vitale et al., 2013).

451   **Chromatin extraction**. Tissues were frozen in liquid nitrogen, pulverized in a press and

452   homogenized using a tissue homogenizer in modified RIPA buffer [25 mM Tris HCl, 7.4; 150

453   mM NaCl ; 5 mM EDTA ; 1% Triton ; 10 % Glycerol ; 50 mM NaF ; 10 mM Na

454   Glycerophosphate] at which the following were added before use [2 mM DTT; 1 mM Na3

455   VO4 ; Protease inhibitor cocktail ; 1 mM PMSF and 1 mM Benzamidine (both from fresh

456   stock in Isopropanol)]. All steps were carried out at 0°C. The extract was clarified at low

457   speed for 5 mn and the resulting supernatant was centrifuged at 10 000 g for 30 mn in a SS34

458   rotor (ThermoFisher, Waltham, MA, USA). Aliquotes of the supernatant were frozen at -80°C

459   for control. Pellet was submitted to sonication (Branson 450D, Danburry, CT, USA) until

460   resuspension. The extract was then submitted to several rounds of French press in order to

461   further homogenize the oyster chromatin. Protein concentration of the chromatin extract was

462   determined using the Bradford assay. Chromatin fractions were frozen at -80°C until further

463   use. Chromatin samples were incubated in Laemmli buffer containing 50 mM Iodoacetate and

464   again submitted to sonication before heating at 94°C for 10 mn. Sample was loaded on a 12%

465   SDS-PAGE and transferred to PVDF membrane (MerckMillipore, Darmstadt, Germany).

466   **Purification of the oyster FLN.** Oyster tissues were frozen in liquid nitrogen and ground to

467   powder in a press. Particular attention was brought to prevent protein degradation since this

468   large protein (323 kDa) is labile. Typically, 30 g of powder were homogenized using a

469   Polytron in 50 mL of 300 mM KCl in buffer A [20 mM Hepes/KOH (7.5); 1 mM MgCl$_2$; 0.1

470   mM EDTA; 10% (vol/vol) Glycerol; 1 mM dithiothreitol; 0.5 mM Phenyl Methyl Sulfonyl

471   Fluoride (PMSF) and 1 x Protease inhibitor cocktail]. The extract was clarified by low speed

472   centrifugation into 50 mL Falcon tubes to pellet remaining tissue fragments. The supernatant

473   was then submitted to 100 000g ultracentrifugation on SW28 rotor (Beckman Coulter,

474   Villepinte, france) at 4°C for 1 hr. The typical concentration for the S100 extract was 10 mg

475   mL^{-1}. All chromatography resins were from GE Healthcare (Fairfield, CT, USA). Briefly, 2

476   mL of a S100 oyster protein extract were incubated in a 20 mL batch of SP Sepharose FF

477   cation exchanger, rinsed with 35 mM KCl in buffer A and eluted with 6 mL of 250 mM KCl

478   in buffer A. Supernatant was diluted to 35 mM KCl in buffer A before injection in Q

479   Sepharose HPLC. After rinse with 35 mM KCl in buffer A, elution was carried out with a

480   linear gradient from 35 to 400 mM KCl in buffer A. The elution peak, detected through

481   absorbance at 280 nm, corresponded to the 250 mM KCl fractions. Analysis of the protein

482   elution peak was done on Coomassie-stained 8% SDS-PAGE. Fractions containing an intense

483   and high molecular weight band over the 250 kDa marker were pooled and diluted to 35 mM

484   KCl in buffer A before injection on SP Sepharose FF cations exchanger and further rinsed

485   with 35 mM KCl in buffer A and eluted with a linear gradient from 35 to 400 mM KCl in

486   buffer A. Fractions of the main peak eluted at 250 mM KCl were pooled and analyzed as

487   above. Positive elution fractions were diluted at 35 mM KCl in buffer A before injection on a

488   heparin Affigel column and rinsed with 35 mM KCl in buffer A. Elution fractions

489   (corresponded to 200 mM KCl) were confirmed to contain the high molecular band as above

490   (Fig. 6A). Positive fractions were precipitated with 70% Ammonium Sulfate at 4°C. Pellet

491   were solubilized in electrophoresis buffer and denatured in Laemmli buffer without ß-

492   mercapto ethanol before electrophoresis on a 7% preparative SDS-PAGE. A unique band over

493   250 kDa was revealed using colloidal blue. The band was cut off the gel and it was analyzed

494   through Mass Spectrometry (Table S4), which provided an unambiguous signature for FLN.

495   **FLN analysis on SYNAPT mass spectrometer**

496   The MS and MS/MS analyzes were performed on the SYNAPT™ an hybrid quadrupole

497   orthogonal acceleration time-of-flight tandem mass spectrometer (Waters, Milford, MA)

498   equiped with a Z-spray ion source and a lock mass system. The capillary voltage was set at

499   3.5 KV and the cone voltage at 35 V. Mass calibration of the TOF was achieved using

500   phosphoric acid (H3PO4) on the [50; 2000] m/z range in positive mode. Online correction of

501   this calibration was performed with Glu-fibrino-peptide B as the lock-mass. The ion (M+2H)

502   2+ at m/z 785.8426 is used to calibrate MS data and the fragment ion (M+H)+ at m/z

503   684.3469 is used to calibrate MS/MS data during the analysis.

504   For tandem MS experiments, the system was operated with automatic switching between MS

505   and MS/MS modes (MS 0.5 s/scan on m/z range [250; 1500] and MS/MS 0.7 s/scan on m/z

506   range [50; 2000]). The 3 most abundant peptides (intensity threshold 60 counts/s), preferably

507   doubly and triply charged ions, were selected on each MS spectrum for further isolation and

508   CID fragmentation with 2 energies set using collision energy profile. Fragmentation was

509   performed using argon as the collision gas. The complete system was fully controlled by

510   MassLynx 4.1 (SCN 566, Waters, Milford, MA). Raw data collected during nanoLC-MS/MS

511   analyses were processed and converted with ProteinLynx Browser 2.3 (Waters, Milford, MA)

512   into .pkl peak list format. Normal background substraction type was used for both MS and

513   MS/MS with 5% threshold and polynomial correction of order 5, and deisotoping was

514   performed.

515   **Image Quantification.**

516 Manual counting of H3P-positive cells (Red) and DAPI (blue) was performed using the

517 analyze/cell counter plugin of the ImageJ software on several confocal images acquired using

518 the x 20 objective. Total H3P-positive cells and total nuclei were summed for each animal.

519 At least 1000 cells were counted for both gill and mantle for each animal (n= 3). Error bars

520 are s.e.m.

521 **Microscopy**. IHC were viewed using a Zeiss Axioimager Z2 (Oberkochen, Germany) with

522 Zeiss 20X Plan Apo 0.8 and Zeiss 40X Plan Apo 1.3 Oil DIC (UV) VIS IR. Micrographs

523 were collected using a Coolsnap HQ2 CCD camera (Roper Scientific, Evry, France) driven by

524 Metamorph 7.1 software (Molecular Devices). Confocal microscopy was performed using a

525 Zeiss LSM780 Confocal with Zeiss 40X PLAN APO 1.3 oil DIC (UV) VIS-IR. Series of

526 optical sections were collected. Histology was viewed using a Nanozoomer (Hamamatsu,

527 Massy, France) to provide both an overview and a detailed structure of GB. Images were

528 analyzed through the NDP view software (Hamamatsu, Massy, France).

529

530

531

538

539

540

541

542

543 **FOOTNOTES**

544 **Author contributions**

545 MJ, NM, PC, JC, JMS and CD performed experiments and analyzed data. CD designed the

546 experiments and wrote the manuscript.

547 **Competing interests**

548 The authors declare no competing interests.

549 **Funding**

553 **Supplementary material**

554

555 **REFERENCES**

556

557 1. Aladaileh, S., Nair, S. V., Birch, D. and Raftos, D. (2007). Sydney rock oyster
558   (*Saccostrea glomerata*) haemocytes: Morphology and function. *J. Invertebr. Pathol.*
559   **96**, 48–53.

560 2. Bayne, B. L. (1990). Phagocytosis and non-self recognition in invertebrates. *J. Comp.*
561   *Immunol.* **40**, 723–731.

562 3. Binesse, J., Delsert, C., Saulnier, D., Champomier-Vergès, M. C., Zagorec, M.,
563   Munier-Lehmann, H., Mazel, D. and Le Roux, F. (2008). Metalloprotease vsm is the
564   major determinant of toxicity for extracellular products of *Vibrio splendidus*. *Appl.*
565   *Environ. Microbiol.* **74**(23), 7108-7117.

566 4. Bodnar, A. (2009). Marine invertebrates as models for aging research. *Exp. Gerontol.*
567   **44**, 477–484.

568 5. Boulanger, N., Bulet, P. and Lowenberger, C. (2006). Antimicrobial peptides in the
569   interactions between insects and flagellate parasites. *Trends Parasitol.* **22**, 262– 268.

570 6. Bureau, D., Hajas, W., Surry, N.W., Hand, C. M., Dovey, G. and Campbell, A. (2002).
571   Age, size structure and growth parameters of geoducks (*Panopea abrupta.*
572   Conrad1849) from 34 locations in British Columbia sampled between 1993 and 2000.
573   *Can. Tech. Rep. Fish. Aquat. Sci.* **2413**, 1-84.

574 7. Butler, P. G., Wanamaker A. D., Scourse , J. D., Richardson, C. A. and Reynolds, D. J.
575   (2013). Variability of marine climate on the North Icelandic Shelf in a 1357-year
576   proxy archive based on growth increments in the bivalve *Arctica islandica*.
577   *Palaeogeogr. Palaeocl.* **373**, 141-151.

578 8. Butt, D. and Raftos, D. (2008). Phenoloxidase-associated cellular defence in the
579   Sydney rock oyster, *Saccostrea glomerata*, provides resistance against QX disease
580   infections. *Develop. Comp. Immunol.* **32**, 299–306.

581 9. Cau, J., Faure, S., Comps, M., Delsert, C. and Morin, N. (2001). A novel p21-
582   activated kinase binds the actin and microtubule networks and induces microtubule
583   stabilization. *J. Cell. Biol.* **155**(6), 1029-1042.

584   10. Cheng, T.C. (1981). "Invertebrates blood cells," in Bivalves, eds A.N. Ratcliffe and
585   F.A. Rowley (London: Academic Press), pp 233–301.

586   11. Cheng, T. (1996). in *The American oyster Crassostrea virginica*, eds Kennedy, V.S.,
587   Newell, R. I. E., Eble, A. F. (University of Maryland System, Trenton), pp 299-326.

588   12. Cheng, T.C. and Rodrick, G.E. (1975). Lysozyme and other enzymes in the
589   hemolymph of *Crassostrea virginica* and *Mercenaria mercenaria*. Comp. *Biochem.*
590   *Physiol*. **52**, 443.

591   13. Cherkasov, A.S., Grewal, S. and Sokolova, I.M. (2007). Combined effects of
592   temperature and cadmium exposure on haemocyte apoptosis and cadmium
593   accumulation in the eastern oyster *Crassostrea virginica* (Gmelin). *J. Therm. Biol*.
594   **32**,162–170.

595   14. Cochennec-Laureau, N., Auffret, M., Renault, T. and Langlade, A. (2003). Changes in
596   circulating and tissue-infiltrating hemocyte parameters of European flat oysters,
597   Ostrea edulis, naturally infected with *Bonamia ostreae*. *J. Invertebr. Pathol.* **83**(1), 23-
598   30.

599   15. Comps, M., Bonami, J. R., Vago, C. and Campillo, A. (1976). Une virose de l'huître
600   portugaise (*Crassostrea angulata* Lmk). *C. R. Hebd. Séanc. Acad. Sci.* **282**, 1991-
601   1993.

602   16. Cuénot, L. (1891). Le sang et les glandes lymphatiques. In: Lacaze-Duthiers H, editor.
603   *Archives de Zoologie Expérimentale et Générale*. Paris: Académie des Sciences.

604   17. dos Santos Souza, S. and Araujo Andrade Z. (2012). The significance of the
605   amoebocyte-producing organ in *Biomphalaria glabrata. Mem. Inst. Oswaldo Cruz*
606   (Rio de janeiro) **107**, 598-603.

607   18. Dragojlovic-Munther, M. and Martinez-Agosto, J. A. (2013). Extracellular matrix-
608   modulated Heartless signaling in Drosophila blood progenitors regulates their
609   differentiation via a Ras/ETS/FOG pathway and target of rapamycin function. *Dev.*
610   *Biol.* **384**(2), 313-330

611   19. Duperthuy, M., Schmitt, P., Garzón, E., Caro, A., Rosa, R. D., Le Roux, F.,
612   Lautrédou-Audouy, N., Got P., Romestand, B. et al.. (2011). Use of OmpU porins for
613   attachment and invasion of *Crassostrea gigas* immune cells by the oyster pathogen
614   *Vibrio splendidus*. *Proc. Natl. Acad. Sci. USA* **108** (7), 2993–2998.

615   20. Eble, A. F. and Scro, R. (1996). in *The American oyster Crassostrea virginica*, eds
616   Kennedy V. S., Newell, R. I. E., Eble, A. F. (University of Maryland System, Trenton),
617   pp. 19-71.

618   21. Eckelbarger, K. J. (1976). Origin and development of the amoebocytes of *Nicolea*
619   *zostericola* (PolychaetaTerebellidae) with a discussion of their possible role in
620   oogenesis. *Mar. Biol.* **36**, 169–182.

621   22. Farley, C. A., Banfield, W. G., Kasnic, J. R. G. and Foster, W. S. (1972). Oyster
622   herpes-type virus. *Science* **178**, 759–760.

623   23. Feng S. Y. and Feng J. S. (1974). The effect of temperature on cellular reactions of
624   Crassostrea virginica to the injection of avian erythrocytes. *J. Invertebr. Pathol.* **23**,
625   22-37.

626   24. Finch, C. E. and Austad, S. N. (2001). History and prospects: symposium on
627   organisms with slow aging. *Exp. Gerontol.* **36**, 593-597.

628   25. Galtsoff, P. S. (1964). in *The American oyster*, ed Udall SL, (US Dept Interior,
629   Washington).

630   26. Goedken, M., Morsey, B., Sunila, I., Dungan, C and De Guise, S. (2005). The effects
631   of temperature and salinity on apoptosis of *Crassostrea virginica* hemocytes and
632   *Perkinsus marinus*. *J. Shellfish Res.* **24**(1), 177–183

633   27. Gonzalez, M., Romestand, B., Fievet, J., Huvet, A., Lebart, M. C., Gueguen, Y. and
634   Bachère, E. (2005). Evidence in oyster of a plasma extracellular superoxide dismutase,
635   which binds LPS. *Biochem. Biophys. Res. Co.* **338**(2), 1089–1097.

636   28. Gonzalez, M., Gueguen, Y., Desserre, G., de Lorgeril, J., Romestand, B. and Bachère,
637   E. (2007a). Molecular characterization of two isoforms of defensin from hemocytes
638   of the oyster *Crassostrea gigas*. *Dev. Comp. Immunol.* **31**, 332–339.

639   29. Gonzalez, M., Gueguen, Y., Destoumieux-Garzón, D., Romestand, B., Fievet, J.,
640   Pugniere, M., Roquet, F., Escoubas, J.M.,Van-denbulcke, F., Levy, O. et al. (2007b).
641   Evidence of a bactericidal permeability increasing protein in an invertebrate, the
642   *Crassostrea gigas* Cg-BPI. *Proc. Natl. Acad. Sci. U.S.A.* **104**, 17759–17764.

643   30. Grigorian, M., Liu, T., Banerjee, U. and Hartenstein, V. (2013). The proteoglycan Trol
644   controls the architecture of the extracellular matrix and balances proliferation and
645   differentiation of blood progenitors in the *Drosophila* lymph gland. *Dev. Biol.* **384**(2),
646   301-312.

647   31. Gueguen,Y., Herpin, A., Aumelas, A., Garnier, J., Fievet, J., Escoubas, J.M., Bulet, P.,
648   Gonzalez, M., Lelong, C., Favrel, P. et al. (2006). Characterization of a defensin from
649   the oyster *Crassostrea gigas*. Recombinant production, folding, solution structure,
650   antimicrobial activities, and gene expression. *J. Biol. Chem.* **281**, 313–323.

651　32. Gueguen, Y., Romestand, B., Fievet, J., Schmitt, P., Destoumieux-Garzón, D.,
652　　　Vandenbulcke, F., Bulet, P. and Bachère, E. (2009). Oyster hemocytes express a
653　　　proline-rich peptide displaying synergistic antimicrobial activity with a defensin. *Mol.*
654　　　*Immunol.* **46**, 516–522.

655　33. Hartenstein, V. (2006). Blood Cells and Blood Cell Development in the Animal
656　　　Kingdom. *Annu. Rev. Cell. Dev. Biol.* **22**, 677–712.

657　34. Itoh, N., Okada, Y., Takahashi, K.G. and Osada, M. (2010). Presence and
658　　　characterization of multiple mantle lysozymes in the Pacific oyster, *Crassostrea gigas*.
659　　　*Fish Shellfish Immunol*. **29**, 126–135.

660　35. Jeong, K.H., Lie and K.J., Heyneman, D. (1983). The ultrastructure of the amebocyte-
661　　　producing organ in *Biomphalaria glabrata*. *J. Dev. Comp. Immunol.* **7,** 217–228.

662　36. Jung, S. H., Evans, C. J., Uemura, C. and Banerjee, U. (2005). The drosophila lymph
663　　　gland as a developmental model of hematopoiesis. *Development* **132**: 2521-2533.

664　37. Kuchel, R., Raftos, D., Birch, D. and Vella, N. (2010). Haemocyte morphology and
665　　　function in the Akoya Pearl Oyster, *Pinctada imbricata*. *J. Invertebr. Pathol.* **105**, 36–
666　　　48.

667　38. Lauffenburger, D.A. and Horwitz, A.F. (1996). Cell migration: a physically integrated
668　　　molecular process. *Cell* **84**, 359–369.

669　39. Liu, K., Jiang, M., Lu, Y., Chen, H., Sun, J., Wu, S., Ku, W. Y., Nakagawa, H., Kita,
670　　　Y., et al. (2013). The multiple roles for Sox2 in stem cell maintenance and
671　　　tumorigenesis. *Cell. Signal*. **25**(5), 1264-1271.

672　40. Lambert, C., Soudant, P., Jegaden, M., Delaporte, M., Labreuche, Y., Moal, J.,
673　　　Boudry, P., Jean, F., Huvet, A. and Samain, J. (2007). *In vitro* modulation of reactive
674　　　oxygen and nitrogen intermediate (ROI/RNI) production in *Crassostrea gigas*
675　　　hemocytes. *Aquaculture* **270**, 413–421.

676　41. Landry, C. D., Kandel, E. R. and Rajasethupathy, P. (2013). New mechanisms in
677　　　memory storage: piRNAs and epigenetics. *Trends Neurosci.* **36**(9), 535-542.

678　42. Loker, E. S. and Bayne, C. J. (2001). Molecular studies of the molluscan response to
679　　　digenean infection. *Adv. Exp. Med. Biol*. **484**, 209–222.

680　43. Luna-Acosta, A., Thomas-Guyon, H., Amari, M., Rosenfeld, E., Bustamante, P. and
681　　　Fruitier-Arnaudin, I. (2011). Differential tissue distribution and specificity of
682　　　phenoloxidases from the Pacific oyster *Crassostrea gigas*. *Comp. Biochem. Physiol. B*
683　　　*Biochem. Mol. Biol*. **159**(4), 220-6.

684   44. Magavi, S.S. and Macklis, J. (2008). Immunocytochemical analysis of neuronal
685   differentiation. *Methods Mol. Biol.* **438**, 345-352.

686   45. McIntosh, L. M. and Robinson, W. E. (1999). Cadmium turnover in the hemocytes of
687   *Mercenaria mercenaria* (L.) in relation to hemocyte turnover. *Comp. Biochem.*
688   *Physiol. C* **123**, 61-66.

689   46. Medhioub, W., Ramondenc, S., Vanhove, A.S., Vergnes, A., Masseret, S., Savar, V.,
690   Amzil, Z., Laabir, M. and Rolland, J.L. (2013). Exposure to the neurotoxic
691   dinoflagellate, *Alexandrium catenella*, induces apoptosis of the hemocytes of the
692   oyster, *Crassostrea gigas. Mar. Drugs* **11**, 4799-4814.

693   47. Minakhina, S., Druzhinina, M. and Steward, R. (2007). Zfrp8, the *Drosophila*
694   ortholog of PDCD2, functions in lymph gland development and controls cell
695   proliferation. *Development* **134**, 2387-2396.

696   48. Morga, B., Arzul, I., Faury, N., Segarra, A., Chollet, B. and Renault, T. (2011)
697   Molecular responses of *Ostrea edulis* haemocytes to an *in vitro* infection with
698   *Bonamia ostreae. Dev. Comp. Immunol.* **35**, 323–333.

699   49. Mount, A. S., Wheeler, A. P., Paradkar, R. P. and Snider, D. (2004). Hemocyte-
700   mediated shell mineralization in the eastern oyster. *Science* **304**, 297–300.

701   50. Parslow, T. G., Stites, D. P., Terr, A. I. and Imboden, J. B. (2001). Medical
702   Immunology (Tenth edition). Los Altos: Lange Medical Publishers.

703   51. Peck, L. S. and Bullough, L. W. (1993). Growth and population structure in the
704   infaunal bivalve *Yoldia eightsi* in relation to iceberg activity at Signy island.
705   *Antarctica. Mar. Biol*. **117**, 235–241.

706   52. Philipp, E. and Abele, D. (2010). Masters of Longevity: Lessons from Long-Lived
707   Bivalves – A Mini-Review. *Exp. Gerontol.* **56**, 55-65.

708   53. Pipe, R. K. (1992). Generation of reactive oxygen metabolites by the haemocytes of
709   the mussel *Mytilus edulis*. *Dev. Comp. Immunol.* **16**, 111–122.

710   54. Prado-Alvarez, M., Flórez-Barrós, F., Méndez, J. and Fernandez-Tajes, J. (2013).
711   Effect of okadaic acid on carpet shell clam (*Ruditapes decussatus*) haemocytes by in
712   vitro exposure and harmful algal bloom simulation assays. *Cell. Biol. Toxicol.*
713   **29**,189–197.

714   55. Pruzzo, C., Gallo, G. and Canesi, L. (2005). Persistence of vibrios in marine bivalves:
715   the role of interactions with haemolymph components. *Environ. Microbiol.* **7**(6), 761–
716   772.

717   56. Ray, M., Bhunia A.S., Bhunia N.S. and Ray, S. (2013). Density shift, morphological
718   damage, lysosomal fragility and apoptosis of hemocytes of Indian molluscs exposed to
719   pyrethroid pesticides. *Fish Shellfish Immunol.* **35**(2),499-512.

720   57. Rink, J. C. (2013). Stem cell systems and regeneration in planaria. *Dev. Genes Evol.*
721   **223**(1-2), 67-84.

722   58. Rolland, J. L., Pelletier, K., Masseret, E., Rieuvilleneuve, F., Savar, V., Santini, A.,
723   Amzil, Z. and Laabir, M. (2012). Paralytic toxins accumulation and tissue expression
724   of α-amylase and lipase genes in the pacific oyster *Crassostrea gigas* fed with the
725   neurotoxic dinoflagellate *Alexandrium catenella. Mar. Drugs* **10**, 2519-2534.

726   59. Rosa, R.D., Santini, A., Fievet, J., Bulet, P., Destoumieux-Garzón, D. and Bachère, E.
727   (2011). Big defensins, a diverse family of antimicrobial peptides that follows different
728   patterns of expression in hemocytes of the oyster *Crassostrea gigas*. *PLoS ONE* **6**,
729   e25594

730   60. Rus, F., Kurucz, E., Márkus, R., Sinenko, S. A., Laurinyecz, B, Pataki, C., Gausz, J.,
731   Hegedus, Z., Udvardy, A., Hultmark , D. et al. (2006). Expression pattern of Filamin-
732   240 in *Drosophila* blood cells. *Gene. Expr. Patterns.* **6**, 928–934.

733   61. Salamat, Z. and Sullivan, J. T. (2008) *In Vitro* mitotic responses of the amebocyte-
734   producing organ of *Biomphalaria glabrata* to extracts of *Schistosoma mansoni*. *J.*
735   *Parasitol.* **94**,1170-1173.

736   62. Schmitt P., Rosa, R.D., Duperthuy, M., de Lorgeril, J., Bachère, E. and Destoumieux-
737   Garzón, D. (2012). The Antimicrobial defense of the pacific oyster, *Crassostrea gigas*.
738   How diversity may compensate for scarcity in the regulation of resident/pathogenic
739   microflora. *Front. Microbiol.* **21**, 160.

740   63. Sokol, N. S. and Cooley, L. (2003). Drosophila filamin is required for follicle cell
741   motility during oogenesis. *Dev. Biol*. **260**, 260-272.

742   64. Sokolova, I.M., Evans, S. and Hughes, F.M. (2004). Cadmium-induced apoptosis in
743   oyster hemocytes involves disturbance of cellular energy balance but no mitochondrial
744   permeability transition. *J. Exp. Biol.* **207**, 3369–3380.

745   65. Sunila, I. and LaBanca, J. (2003). Apoptosis in the pathogenesis of infectious diseases
746   of the eastern oyster *Crassostrea virginica. Dis. Aquat. Organ.* **56**(2), 163-70.

747   66. Turekian, K. K., Cochran, J. K., Kharkar, D. P., Cerrato, R. M., Vaisnys, J. R.,
748   Sanders, H. L., Grassle, J. F. and Allen, J. A. (1975). Slow growth rate of a deep-sea
749   clam determined by 228Ra chronology. *Proc. Natl. Acad. Sci. USA* **72**, 2829–2832.

750   67. Vitale, I., Jemaà, M., Galluzzi, L., Metivier, D., Castedo, M. and Kroemer, G. (2013).
751   Cytofluorometric assessment of cell cycle progression. *Methods Mol. Biol*. **965**, 93-
752   120.

753   68. Vogt, G. (2012). Hidden treasures in stem cells of indeterminately growing bilaterian
754   invertebrates. *Stem. Cell. Rev.* **8**(2), 305-317.

755   69. Wanamaker, A. D., Butler, P. G., Scourse, J. D., Heinemeier, J., Eiríksson, J.,
756   Knudsen, K. L. and Richardson, C. A. (2008). Very long-lived mollusks confirm 17th
757   century AD tephra-based radiocarbon reservoir ages for North Icelandic shelf waters.
758   *Radiocarbon* **50**, 399-412.

759   70. Watt, F. M. and Huck, W. T. S. (2013). Role of extracellular matrix in regulating stem
760   cell fate. *Nat. Rev. Mol. Cell. Biol*. **14**, 467-473.

761   71. Xue, Q., Hellberg, M.E., Schey, K. L., Itoh, N., Eytan, R.I., Cooper, R.K. and
762   LaPeyre, J. F. (2010). A new lysozymef rom the eastern oyster, *Crassostrea virginica*,
763   and a possible evolutionary pathway for i-type lysozymes in bivalves from host
764   defense to digestion. *BMC Evol. Biol.* **10**, 213.

765   72. Yao, C.L. and Somero, G.N. (2012). The impact of acute temperature stress on
766   hemocytes of invasive and native mussels (*Mytilus galloprovincialis* and *Mytilus*
767   *californianus*): DNA damage, membrane integrity, apoptosis and signaling pathways.
768   *J. Exp. Biol*. **15**, 4267-77.

769   73. Zhang, G., Fang, X., Guo, X., Li, L., Luo, R., Xu, F., Yang, P., Zhang, L., Wang, X.,
770   et al. (2012). The oyster genome reveals stress adaptation and complexity of shell
771   formation. *Nature* **490**, 49–54.

772   74. Ziuganov, V., San Miguel, E., Neves, R. J., Longa, A., Fernández, C., Amaro, R.,
773   Beletsky, V., Popkovitch, E., Kaliuzhin, S. and Johnson, T. (2000). Life span variation
774   of the freshwater pearl shell: a model species for testing longevity mechanisms in
775   animals. *AMBIO* **29**, 102–105.

776

777

778

779

780

781

782   **Abbreviations**

783   BrdU, Bromodeoxyuridine, ECM, extracellular matrix, FLN, Filamin, IFS, irregularly folded

784   structures, SOD, Superoxide dismutase

785

786

787

788

789

790   **FIGURE LEGENDS**

791   **Fig. 1**. Detail of an IFS region. **A**. Scanning at low magnification shows the presence of

792   stacks of tubules (Tu) and convoluted structures (CS). Higher magnification (insets) revealed

793   nuclei intensely stained with hematoxylin and surrounded with a thin and barely detectable

794   eosin stained cytoplasm. Note that nuclei are packed in the ECM of the epithelium and at the

795   extremities of the tubules. **B**, **C**. Details of convoluted structures at higher magnification **B.**

796   Small pear-shaped cells (inset, arrow) were seen burgeoning out of the ECM (E) into the

797   hemolymph. **C**. Long cytoplasmic extension of stem-like cells (inset, arrow) in the

798   hemolymph of a tubule, in contact with the ECM (E). CS convoluted structures, Tu tubules, E

799   ECM.

800

801   **Fig. 2.** Intense DNA replication in IFS. **A, B.** Tissue was incubated for 16 hrs with BrdU in

802   oyster cell culture before fixation and IHS. **A.** Fluorescent microscopy at low magnification

803   revealed a widespread and intense BrdU labeling in IFS (1-2) and in a few areas of the

804   regularly folded gill (3-4). Higher magnification of a filament vessel (V, white outline)

805   containing BrdU labeled cells (Bar, 25 µm) (5). No BrdU detection in control section (6). **B.**

806   Tissue section treated as above and with cytoplasm staining (green, Alexa 488-Phalloidin).

807   Confocal image reveals that small stem-like cells (arrow head) and large hemocyte-like cells

808   (arrow) are labeled with BrdU in a gill vessel (V, white outline). Arrow head, stem-like cell,

809   arrow, hemocyte-like cell, CR, chitine rod; Phall., phalloidin; V, vessel.

810

811   **Fig. 3**. DNA replication in stem-like cells inside a tubule lumen. Images were acquired by

812   Confocal microscopy of tissue cross-sections after incubation with BrdU (25µM), fixation

813   and IHC using BrdU mAb and Alexa 488-Phalloidin for cytoplasm visualisation. **A**.

814   Observation after a 16 hr BrdU-incubation revealed masses of cells dislaying BrdU-labeling

815   and a thin phalloidin-labeled cytoplasm inside the tubule lumen. **B**. Observation at higher

816   magnification (box in panel A) shows a mass of oblong stem-like cells in the tubule lumen

817   (Continuous and dotted lines delimit a tubule and its lumen, respectively), which are lined up

818 (Panel Phall., dotted line). **C**. Observation of an IFS section showing a vessel (V, delimited by
819 white lines) after a short (2 hrs) BrdU-labeling. Note that the small cells with a thin cytoplasm
820 are BrdU-labeled (arrow heads) while the larger hemocyte-like cells are not (arrows). Ep
821 epithelia, Lu lumen, V vessel.

822

823 **Fig. 4**. Mitoses in the oyster gill and mantle tissues. Cross-sections were submitted to IHC
824 using a rabbit anti-H3P antibody (red) and DAPI (blue) and were analyzed through Confocal
825 microscopy. **A.** Image of a section of the mantle that reveals a few H3P-labeled cells (red) in
826 this tissue, which is essentially made of a few scattered large cells. **B**. Image of a section of
827 the regularly folded gill showing a high density of nuclei (DAPI) of which a fair proportion
828 are H3P-positive (red). **C**. Image of a control gill section treated as above while no anti-H3P
829 antibody was used. **D and E.** Quantification of the H3P-labeled cells in mantle and gill
830 sections. Counting was done on at least 1000 nuclei on representative views for each animal
831 (n=3). **D.** Mitotic index in the oyster gill and mantle. The percentage of mitotic nuclei is
832 21.7 % and 4.7% in gill and mantle, respectively. **E.** Density of mitotic nuclei per $100\mu m^2$.
833 The density of mitotic nuclei is much higher in the gill (0.192 +/- 0.034) than in the mantle
834 (0.005 +/- 0.0009).

835

836 **Fig. 5**. Abundance of precursor cells in the IFS. Images acquired through fluorescence (**C**) or
837 confocal microscopy (**A**, **B**, **D**) following IHC using a rabbit Sox2 antibody (red) and DAPI
838 (blue). **A**. Numerous IFS epithelial cells are Sox2-positive. Please not that long cytoplasmic
839 extensions as described on Fig. 1 C (inset) are occasionally decorated with Sox2. **B**. At higher
840 magnification, Sox2 decorates the nucleus of gill epithelial cells as well as the cytoplasm of a
841 few small teardrop shaped cells similar to the stem-like cells on Fig. 1B (inset). **C**. Groups of
842 Sox2-labeled cells (stars) loosely associated inside the hemolymph lumen (Lu, outlined in
843 white) of an IFS tubule. **D**. Tissue section treated as above but without primary Sox2 antibody.
844 Ep epithelium, Lu lumen.

845

846 **Fig. 6**. Small cells displaying markers for stemness and for hemocytes in the IFS. **A**.
847 Hemocyte progenitors co-stained with Sox2 and SOD. IHC was carried out using a rabbit
848 Sox2 antibody (red), a mouse SOD antibody specific for hemocytes (green) and DAPI (blue).
849 IFS structure composed of several layers of Sox2-positive cells in the tubules region (Tu)
850 whereas SOD-positive cells, the hemocytes, are essentially located in a nearby vessel (V,
851 white outline). Similarly, cells co-labeled for Sox2 and SOD (stars) are mostly located in the

852 vessel (V), which suggests that progenitor cells may differentiate into hemocytes as they

853 move towards the vessel (see also Fig. S5). **B**. Precursor cells replicate DNA and differentiate

854 into hemocytes in the gill. A 10 mm-thick cross-section of the gill was incubated with 25 µM

855 BrdU for 16 hrs before fixation and IHC. BrdU-labeled DNA (blue) and FLN (red) were

856 revealed as described above. Fluorescent microscopy revealed an abundance of large cells

857 labeled for BrdU and FLN in the hemolymph of a main vessel (V) at the base of the gill. **C**.

858 High magnification of B Box. FLN-stained cells harbor a typical punctuated nuclear BrdU-

859 labeling. Ep epithelium, Tu tubules, V vessel.

860

861

862 **SUPPLEMENTARY FIGURE LEGENDS**

863 **Fig. S1.** General structure of the oyster gill. **A**. Oyster gills are both made of two V-shaped

864 demi-branches each composed of an ascending and a descending lamella delimiting a water

865 tube and linked by inter-lamellar junctions. **B**. Each lamella is a succession of folded

866 structures, termed plicas, which are made of the repetition of a tubular structural unit called

867 filament. The central part of the filament is occupied by a sinus, a space filled with

868 hemolymph, while the basal part of the filament consists of a more or less regular layer of

869 tightly-packed and non-ciliated cells usually referred to as epithelium. **C**. Hematoxylin/eosin

870 stained cross-section of the oyster gill and its attachment region scanned at low magnification

871 using a Nanozoomer (Hamamatsu, Massy, France). Id inner demi-branch, IFS irregularly

872 folded structure, Il inter-lamellar junction, M mantle, Lg left gill, Od outer demi-branch, Rg

873 right gill. Credit for the drawings to Maryland Sea Grant, The American oyster *Crassotrea*

874 *virginica*, editors: VS Kennedy, RIE Newell, AF Eble, Mechanisms and physiology of

875 feeding, RIE Newell and CJ Langdon, illustrated by D Kennedy, modified from Galtsoff

876 (1964).

877 **Fig. S2.** Relative BrdU incorporation in the oyster gill and mantle cells. Oysters were injected

878 with BrdU (n= 3) or seawater (controls, n= 3) into the sinus of the adductor muscle. The

879 animal body was fixed in Davidson's fixative 16 hours later. Fluorescence micrographs were

880 recorded at low magnification (x 20) in the Cy3 channel for BrdU while the GFP channel is

881 used to outline the tissues through autofluorescence (AF). Images (A, C, E) are representative

882 of the BrdU-injected animals (n= 3) and (B, D, F) of the control animals (n=3) **A.** BrdU-

883 labeling appears evenly spread in IFS section. (Inset). Intense and punctuated BrdU-labeling

884 shown at higher magnification. Inset scale bar, 20 µm. **B.** No BrdU signal on this IFS section

885 from a control oyster injected with seawater. **C.** Labeling of a region of the regularly folded

886   gill. **D.** No BrdU signal on section of the regularly folded gill from a control oyster injected

887   with seawater. **E.** BrdU labeling of a mantle area including a large vessel (V) section. A few

888   scattered positive cells appear on the vessel vicinity. **F.** No BrdU signal on this section of the

889   mantle from a control oyster injected with seawater. V vessel.

890   **Fig. S3**. FACS analysis of the cell cycle distribution of the oyster gill and mantle cells. Gills

891   and mantles from oysters (n= 6) were minced and digested with Pronase in Hank's buffer for

892   dissociation into individual cells. Cells were fixed and DNA was stained with propidium

893   iodide (PI). **A.** Samples were analyzed through Flow Activated Cell Sorting. The gating

894   procedure to isolate a population of individual cells consists in sequentially separating events.

895   Cells were sorted through a normal light scattering to exclude bacteria and debris (granularity

896   versus size; left panel) (50.000 to 44.600 events). Then fluorescent cells were gated according

897   to their size in order to exclude doublets (central panel) (44.6000 to 38.200 events). Gated

898   populations of fluorescent cells are figured according to their cell cycle profile (right panel),

899   the peak of replicative cells corresponding to S and G2/M. **B.** Cell cycle profiles for gill and

900   mantle, which are representative of the data obtained through 5 independent experiments.

901   Green peak, replicative cells. **C.** Percentage of replicative cells in the gill and mantle cells,

902   which are 17.3% +/-5 and 7.2% +/-3 for gills and mantles (n=6), respectively. Results are

903   reported as means +/- SD. * $p < 0.01$(two-tailed Student's t-test).

904

905   **Fig. S4.** Antibody specificity for oyster proteins. Immunoblots were carried out against oyster

906   chromatin (A) or tissue extracts (B and C) (50 and 10 µg of total proteins, respectively)

907   transferred to PVDF membrane. **A.** H3P rabbit antibody revealed a unique band for histone

908   H3 (15 kDa) on oyster chromatin extract (Chr) while no band was detected on the cytosolic

909   extract (Sup). **B.** Rabbit Sox2 antibody revealed a unique band (36 kDa) of the predicted

910   molecular weight for Sox2 (EKC24855) on protein extract. **C**. An in-house immuno–purified

911   FLN rabbit antibody revealed a unique band migrating well over the 250 kDa marker in

912   agreement with the predicted molecular weight for the oyster FLN (323 kDa; EKC28512).

913

914

915   **Fig. S5**. Precursor cells differentiate into hemocytes in the oyster gill. Confocal images of the

916   tubules (**A**) and convoluted structures (**B**) of an IFS region using Sox2 (red) and SOD (green)

917   antibodies and DAPI (blue). Sox2-labeled cells are essentially in the tubules region while

918   SOD-labeled cells are essentially in the underlying connective tissue (Co) and vessels (V,

919   white outline). Cells co-labeled for Sox2 and SOD are located in the underlying connective

920   tissue (Co) under the tubules (Tu) and in the neighboring vessel (V). Co connective tissue, V

921   vessel, Tu tubule.

922   **Fig. S6**. Filamin antibody specificity for a sub-population of hemocytes. **A.** Oyster FLN was

923   purified to homogeneity on FPLC. An aliquote of a purified fraction was electrophoresed on a

924   7% SDS-PAGE. Colloidal Coomassie staining revealed a unique band (panel 1) migrating

925   well above the 250 kDa marker (Thermofisher, Waltham, MA, USA). Western blot using an

926   in-house immuno-purified rabbit FLN antibody (FLNAb) revealed a unique band (panel 2)

927   corresponding to the Coomassie stained band. **B.** Oyster cross-section encompassing the

928   gonad submitted to IHC using FLNAb (red) and DAPI (blue). Axillary cells surrounding the

929   oocytes were specifically and intensely labeled for FLN. Autofluorescence (Alexa 488) to

930   outline the tissue structures. **C.** Tissue sections stained using the FLN (red) and SOD antibody

931   (green) and DAPI (blue). Image on confocal microscopy of hemocytes in a gill vessel. FLN

932   (red) strongly stained the cytoplasm of a sub-population of hemocytes also stained for SOD

933   (green). **D.** Confocal image of a tissue section treated as in B and C but with no primary
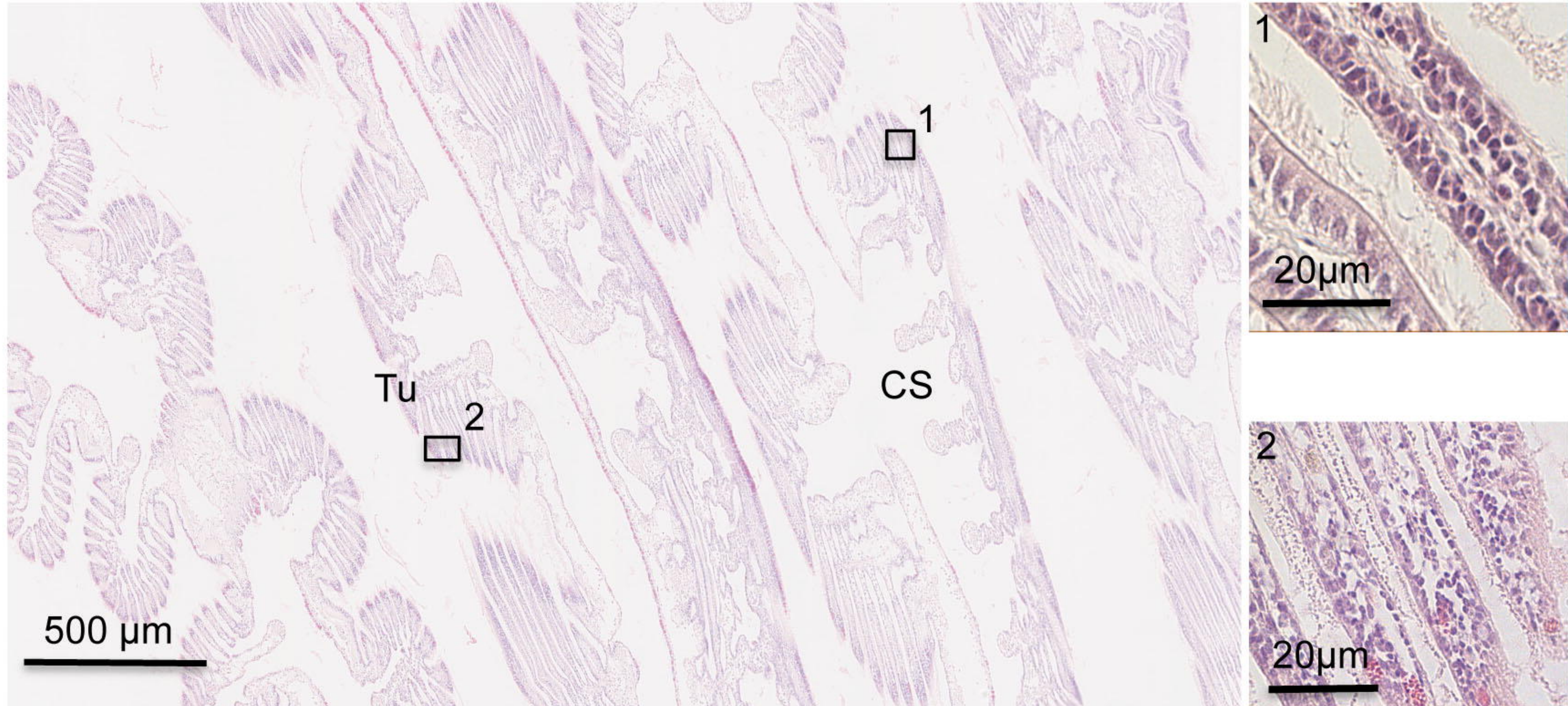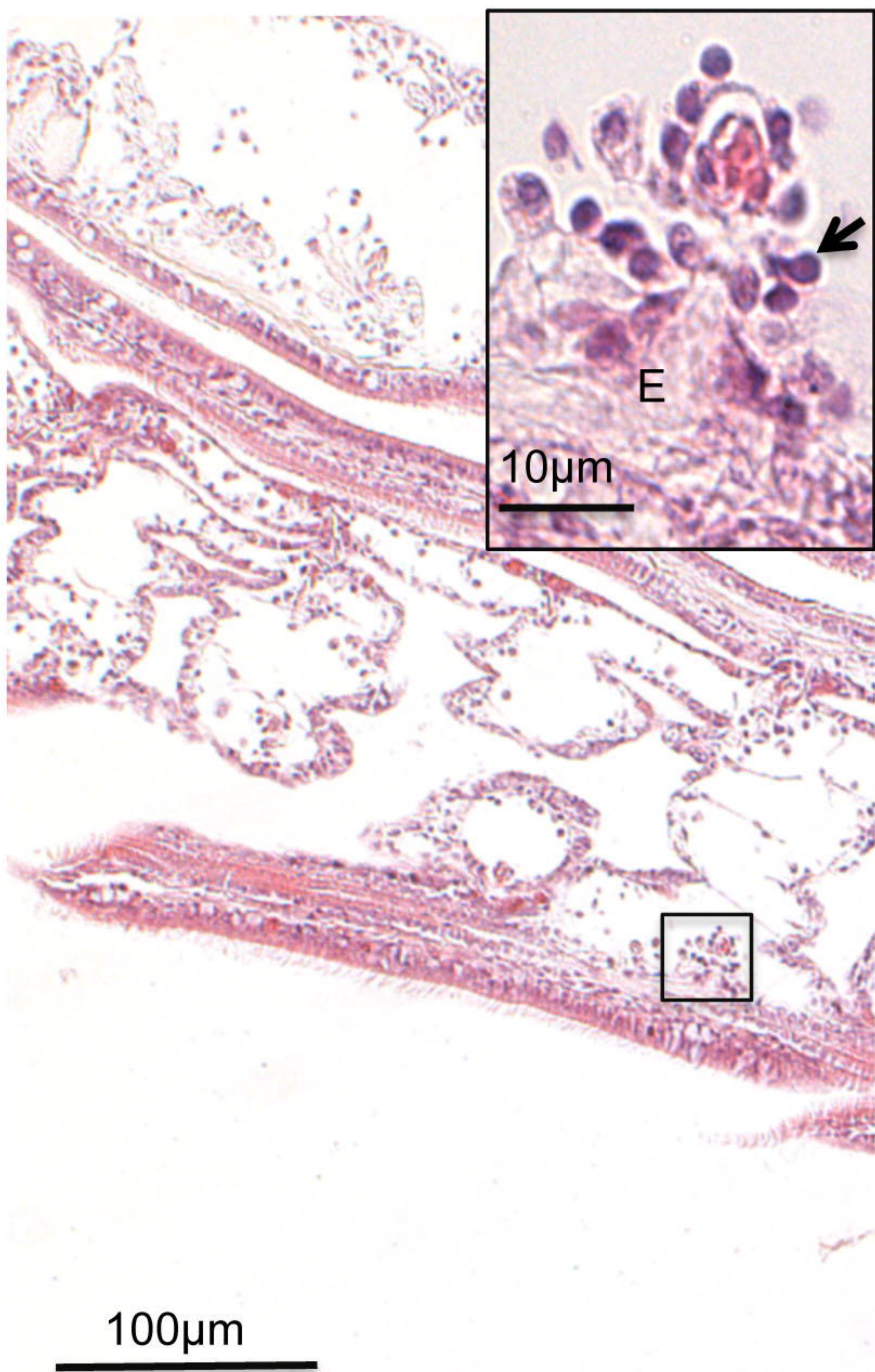
934   antibodies.

935   **Table S1.** FACS analysis of the DNA content of oyster gill and mantle cells.

936   **Table S2.** Counting of the H3P-positive nuclei on representative regions of the mantle.

937   **Table S3.** Counting of the H3P-positive nuclei on representative regions of the gill.

938   **Table S4**. MS/MS data interpretation. The peak list has been searched against a

939   UniProtKB/Swiss-Prot database of *Crassostrea gigas* combined target-decoy database

940   (created 2013-07-30, containing 26945 target sequences plus the same number of reversed

941   decoy sequences) using Mascot (version 2.4.1, Matrix science, London, England). The

942   database contained sequences of human proteins including common contaminants (human

943   keratins and porcine trypsin) and was created using an in-house database generation toolbox

944   (http://msda.u-strasbg.fr). This analysis unambiguously identifies the purified protein as the

945   oyster FLN.

946

A

1

2

3

100 µm

4

V

5

Ep   CR

V

V

6

B   BrdU

50µm

Phall.

Merge

V

A

BrdU   Phall.   Merge

50µm

B

Ep
Lu
Ep

20µm

C

BrdU
Ep
V
Ep

20µm

Phall

Merge

Columns labeled: DAPI, Sox2, Merge

Panel A: scale bar 20μm

Panel B: scale bar 5μm

Panel C: labels Lu, Ep, Ep; scale bar 50μm

Panel D: scale bar 50μm

A

| Sox2 | DAPI | SOD | Merge |

30µm

B

| FLN | BrdU | Merge |

50 µm

C

10µm